

Probabilistic Verification for Reliability of a Two-by-Two Network-on-Chip System

Riley Roberts¹[0000-0002-8676-3767], Benjamin Lewis¹[0000-0003-2968-0233],
 Arnd Hartmanns²[0000-0003-3268-8674], Prabal Basu³[0000-0002-4860-1089],
 Sanghamitra Roy¹[0000-0002-3927-1612], Koushik
 Chakraborty¹[0000-0003-0228-2737], and Zhen Zhang¹[0000-0002-8269-9489]

¹ Utah State University, Logan, UT, USA

{riley.roberts, benjamin.lewis}@aggiemail.usu.edu, {koushik.chakraborty,
 sanghamitra.roy, zhen.zhang}@usu.edu

² University of Twente, Enschede, The Netherlands a.hartmanns@utwente.nl

³ Cadence Design Systems, CA, USA bprabal@cadence.com

Abstract. Modern network-on-chip (NoC) systems face reliability issues due to process and environmental variations. The power supply noise (PSN) in the power delivery network of a NoC plays a key role in determining reliability. PSN leads to voltage droop, which can cause timing errors in the NoC. This paper makes a novel contribution towards formally analyzing PSN in NoC systems. We present a probabilistic model checking approach to observe the PSN in a generic 2x2 mesh NoC with a uniform random traffic load. Key features of PSN are measured at the behavioral level. To tackle state explosion, we apply incremental abstraction techniques, including a novel probabilistic choice abstraction, based on observations of NoC behavior. The MODEST TOOLSET is used for probabilistic modeling and verification. Results are obtained for several flit injection patterns to reveal their impacts on PSN. Our analysis finds an optimal flit pattern generation with zero probability of PSN events and suggests spreading flits rather than releasing them in consecutive cycles in order to minimize PSN.

Keywords: Probabilistic Model Checking, Network-on-Chip, Formal Methods, Abstraction

1 Introduction

As the complexity advances in designing reliable distributed many-core systems, *network-on-chip* (NoC) has become the de-facto standard for on-chip communication. In general, their architecture composes of topologically homogeneous routers operating synchronously in a decentralized manner, and communication is governed by a predefined routing protocol. While sharing similarity with conventional computer networks, a NoC design faces unique reliability challenges, such as process and environmental variations. Precise evaluation of the NoC

early in the design flow is paramount to establish rigorous reliability and performance guarantees. NoC reliability analysis has to capture and quantify the design’s inherent distributive and reactive characteristics.

Existing literature lacks probabilistic verification of the NoC. Formal verification of the NoC has focused primarily on functional correctness [1–5], checking performance [6–8], and security [9, 10]. Advances in formal verification of probabilistic systems have produced mature tools such as the MODEST TOOLSET [11], which includes the MCSTA probabilistic model checker and the MODES statistical model checker [12], Storm [13], and PRISM [14]. However, these existing works have not focused on the NoC domain.

Building on the previous success in the probabilistic verification of a NoC central router [15], we present probabilistic verification of the *power supply noise* (PSN) for a 2x2 mesh NoC system and its impact on the system’s reliability under uniform random traffic loads. We cumulatively apply abstraction techniques to tackle state space explosion for a 2x2 mesh NoC model. This includes a novel abstraction technique based on changing probabilistic choices derived from critical observations under design constraint assumptions. Verification results show significant scalability of our abstraction techniques, which reduce the state space growth from exponential to polynomial. They reveal extremely low PSN activity in the 2x2 NoC under an every other clock cycle flit injection pattern, while showing relatively high PSN under a burst style flit injection. This indicates the large impact design decisions have on PSN. Additionally, we report on an efficient flit generation pattern that incurs *zero* probability for PSN events and make recommendations for flit generation patterns to minimize PSN.

2 Motivation

PSN in the power delivery network of an integrated circuit is composed of two major components: (a) resistive noise—the product of the current drawn and the lumped resistance of the circuit ($i \times r$); and (b) inductive noise—proportional to the rate of change of current through the inductance of the power grid ($\frac{\Delta i}{\Delta t}$). For a distributed system such as a NoC, the latter plays a central role [16].

A high inductive noise is responsible for the intermittent peaks in the cycle-wise noise profile of a NoC. This noise is substantially growing with technology scaling. It has been recently shown that in an 8x8 NoC, the peak PSN can increase from 40% of the supply voltage at the 32-nm technology node to about 80% of the supply voltage at the 14-nm technology node, while running a uniform-random synthetic traffic pattern [16]. Such a droop can radically degrade the delay of various on-chip circuit components causing timing errors in the pipe-stages of the NoC routers. Hence, PSN worsens the reliability and performance of the on-chip communication.

Existing approaches to mitigate PSN are a far cry from a truly reliable NoC design paradigm that can be deployed in mission-critical systems, as they do not guarantee the worst-case peak PSN [16, 17]. These works do not provide any bounds on the temporal PSN profile for a router, given an application execution.

Hence, temporal high peak PSNs may still exacerbate the NoC reliability across different operating conditions. To address this critical reliability challenge, we show that probabilistic verification can offer precise bounds on the performance and reliability of the NoC. Our proposed techniques will lead the way to future reliable NoC designs.

3 Concrete Formal Model for NoC

This work analyzes the synchronous 2x2 mesh NoC shown in Figure 1. There are four symmetric routers, each with three incoming channels: one in the horizontal X direction, one in the vertical Y direction, and a local channel. Each channel has a buffer with the capacity of storing four network flits. Each router has an arbiter which resolves conflicts, i.e., multiple input flits competing for the same output direction, and forwards the winning flit in one clock cycle. The arbiter uses Round-Robin protocol to resolve multiple simultaneous requests to ensure fairness in each direction. The NoC uses X-Y routing, where a flit is first routed in the X direction until it is at the destination router or in the same column as the destination. It is then routed in the Y direction to the destination. For example, in Figure 1, if router 0 were to receive a flit destined for router 3 on the local channel, the flit would be sent first in the X direction to router 1, then in the Y direction to router 3.

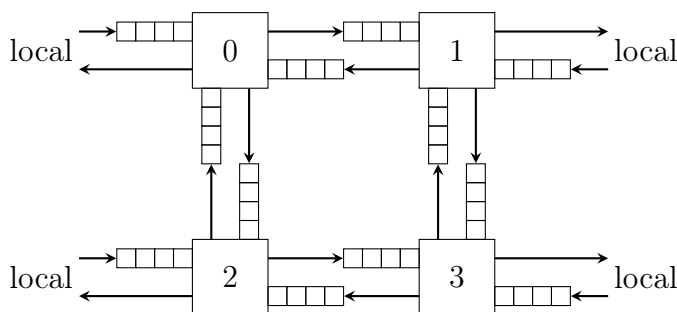


Fig. 1: Architecture of the 2x2 NoC model.

When a new flit is generated in each router’s local channel, its destination is uniformly randomly selected among the other three routers. The routers then route all flits simultaneously. First, a flit’s next forwarding direction is determined by the X-Y routing protocol by comparing its destination and the current router. The arbiter then forwards the flit to the neighboring router and resolves conflicts if they arise. We use a priority queue in the arbiter to implement the Round-Robin scheduling mechanism in order to maintain fairness when resolving conflicts. Figure 2 illustrates how the priority queue works. When two channels conflict, the one closer to the front of the priority queue is serviced by the arbiter

and the other is marked as unserved. A channel that fails to send due to the receiving buffer being full is also marked as unserved. At the end of the current clock cycle, the priority queue updates by shifting all unserved channels to the front of the queue and pushing those served to the end, while maintaining their relative ordering. We use the high-level formal modeling language MODEST [11] to specify the probabilistic NoC model in Figure 1.

Data types of the concrete NoC model are shown in Listing 1.1. The buffers are modeled as a FIFO queue with a capacity of four. Each channel is modeled as a datatype containing a buffer, the channel’s priority, the forwarding direction for the flit at the front of the queue, the ID of the channel, and a Boolean variable indicating whether the channel was served or not. Each router is modeled as a datatype with an array of three channels, the order of which determines the priority, and two counters `unserved` and `totalUnserved` that keep track of the number of unserved channels and are used by the arbiter. The NoC model has an array of four routers.

Listing 1.1: Channel and router datatypes.

```
datatype channel = {int direction ,
                    int id, bool served, int priority ,
                    queue buffer};
datatype router = {int unserved,
                  int totalUnserved, channel[] channelArray};
```

The two components of PSN are modeled as follows. Resistive noise is measured by accumulating the clock cycles where there is high router activity, i.e., all three buffers in a router are able to forward flits. This is represented by a variable *resistiveNoise*, which increments every time a router encounters a cycle with high activity. Inductive noise is measured by accumulating clock cycles where there is a high rate of change of current draw. This directly corresponds to cycles where a router switches between forwarding all flits to forwarding no flits and vice versa. Represented by the variable *inductiveNoise*, it increments on the cycles of abrupt change in router activity.

The relation between the two PSN components, *resistiveNoise* and *inductiveNoise*, and their associated real-world applications is discussed in [16, 18]. We rely on the analysis presented there as the foundation. The purpose of specifying and checking these properties is to understand the likelihood of PSN at a behavioral level under a given routing protocol. The intermittent peaks in the cycle-wise noise profile of the NoC is strongly correlated to the NoC router activities. Hence, understanding PSN behaviorally can help with the design of routing protocols and other higher-level NoC designs independent of the physical hardware implementation of the NoC.

4 Need for Abstraction

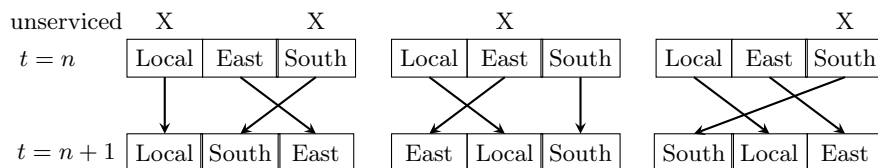


Fig. 2: Three priority queue examples.

The state spaces of all probabilistic formal models presented in this work are large *discrete-time Markov chains* (DTMC), and they are analyzed by the tools in the MODEST TOOLSET, namely, MCSTA and MODES. The concrete model presented in the previous section incurs an exponential state space growth as the number of considered clock cycles increases. This is due to the combinations of flits in all twelve buffers in the model. To address this issue, we investigate several abstraction techniques. These abstraction techniques are performed *cumulatively*: results labeled using the name of one technique are the results of that technique applied on top of all previous abstractions.

4.1 Predicate Abstraction to Simplify Complex Data Structures

Predicate abstraction is applied first to the concrete model. It works by formulating predicates that capture critical decision points in the concrete model, and then transforming the model to include only predicate variables. In our model, the predicate abstraction converts all complex data structures into predicate variables. For example, the two predicate variables in Listing 1.2 are defined as the two possible forwarding directions of the front flit in the local channel buffer of router 0. Performing predicate abstraction in this manner significantly simplifies the complex data structures in the concrete model, and it also preserves the properties *resistiveNoise* and *inductiveNoise*, since router and arbiter activity remain unchanged after abstraction. Note that predicate abstraction is only applied to simplify complex data structures in our concrete model to turn them into predicate variables, instead of the entire concrete model. Therefore, it does not introduce nondeterministic behavior as a result. Unfortunately, the predicate abstracted model still incurs significant state space explosion with 7 or more clock cycles.

Listing 1.2: Example predicate variables after predicate abstraction.

```
bool r0L1;//noc[0].channel[local].direction==east
bool r0L2;//noc[0].channel[local].direction==south
```

4.2 Probabilistic Choice Abstraction

Next, we present a novel *probabilistic choice abstraction* technique. The idea comes from the following observation. The flit's destination is selected by a

uniform random distribution when it is input into the local buffer of each router, but the destination information is not checked *until* the flit enters the router, where it is used to decide the flit forwarding direction. This implies that, when generating states, enumeration of all possible values for the destination variable does not need to happen at its initial assignment, but can be delayed until the location where its value is first checked. Furthermore, the destination variable is not in use beyond this point. Consequently, this variable can be entirely replaced by a probabilistic choice when its value is evaluated, i.e., when the router decides the flit’s direction, while preserving the model behavior. The noteworthy state reduction comes from delaying the enumeration of all of the possible values until it is evaluated. This idea is similar to the concept of *constant propagation* in compiler optimization.

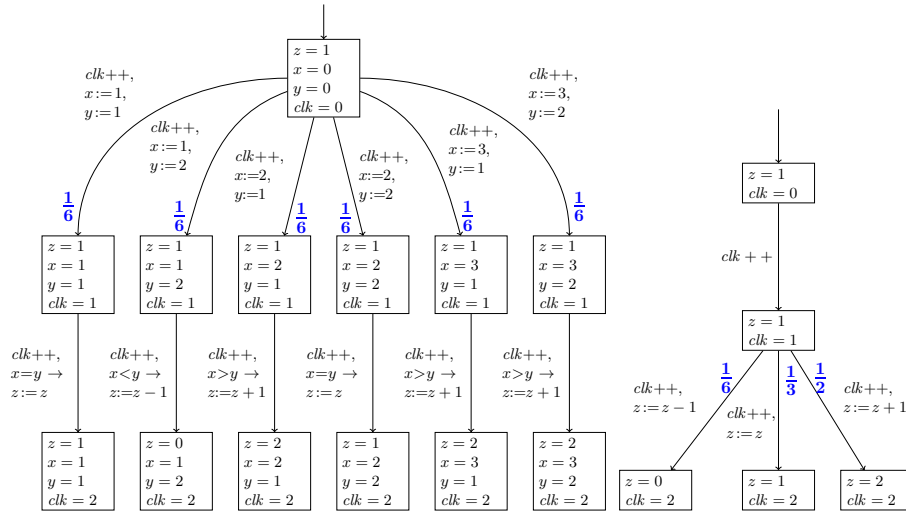


Fig. 3: Probabilistic Choice Abstraction

Figure 3 compares state graphs for an illustrative model before and after applying probabilistic choice abstraction. The left one is the fully expanded state space of a concrete model, which determines the update of z by comparing two uniform random integer variables $x \in [1, 3]$ and $y \in [1, 2]$. This results in six unique states when the clock reaches 2. Variables x and y are only compared at this row, but not evaluated in any of the six states in the middle row, and are not used after the comparison. Thus, we can apply probabilistic choice abstraction by replacing x and y with a probabilistic choice with explicit probabilities as the state graph on the right illustrates. The abstract model creates only five states and preserves the behavior of the observable variables z and clk .

Figure 3 is similar to our predicate-abstracted NoC model. In this figure, the observable variables are z and clk . Variables x and y are just used to de-

termine the behavior of z . Similarly in our model, the observable variables are *resistiveNoise*, *inductiveNoise* and *clock*. All other variables are used to determine the update behavior of *resistiveNoise* and *inductiveNoise* in between clock cycles. The destinations of the flits are the only probabilistically updated variables in the model. Using this abstraction, we are able to remove the destination variables from the state space, and replace them with a probabilistic choice. This abstraction preserves the behavioral activities of the flits, which determine *resistiveNoise* and *inductiveNoise*. We are currently working on developing theories and proofs for this abstraction technique. We have experimentally observed that for as many cycles as the concrete and abstract models can run, the behaviors of *resistiveNoise* and *inductiveNoise* are identical across the concrete, predicate abstract, and probabilistic choice abstract models.

Probabilistic choice abstraction can be directly applied to a formal model without first generating the state graph of the concrete model. This idea is applied to the NoC model in the following way. Any flit coming from the local channel in router 0 can be destined for router 1, 2, or 3 as shown in Figure 1. Given that the NoC uses X-Y routing and uniform random distribution of destinations, if the destination is router 1 or 3, the flit is forwarded east with probability $\frac{2}{3}$. If the destination is router 2, the flit is forwarded south with probability $\frac{1}{3}$. Any incoming flit coming from the east buffer of router 0 must have been generated in router 1 and is destined for either router 0 or router 2 with equal probability $\frac{1}{2}$. Similarly, any incoming flit in the south buffer of router 0 is generated by either router 2 or 3, and can only be destined for this router. Due to the symmetric nature of the NoC, this same pattern is true for all routers. Because the exact destination of the flit is no longer required knowledge, the buffers can be further abstracted as detailed in the next section.

4.3 Boolean Queue Abstraction

With three buffers in each router, there are a total of six possible orders that determine the priority in servicing each buffer in the case of conflict. Our analysis indicates that, for the 2x2 NoC with X-Y routing, the north/south buffer can *never* be in conflict with the local buffer. Therefore, the model only needs to keep track of the local and north/south buffers priority relative to the east/west buffer but not to each other. This allows us to abstract the six possible orders into four, further reducing the state space.

Further, because all buffers operate as FIFOs, an empty buffer element can only exist either after a non-empty element if the buffer is neither full nor empty, or at the front of the buffer if the buffer is empty. Rather than keep track of the buffer's contents, we only need the length of flit occupancy in a buffer, i.e., the number of non-empty elements. This length is represented as a bounded integer ranging between 0 and 4. In general, a buffer storing maximally n Boolean variables incurs 2^n states, but only $n + 1$ states if its occupancy is recorded. In order to maintain correct behavior through this abstraction, the four arbiter processes were synchronized on one action, rather than run sequentially.

Figure 4 depicts the decision procedure in a router after Boolean queue abstraction. It first checks for a possible conflict by checking if the east/west buffer is empty. If the buffer is not empty (i.e., `ewLen` \neq 0), the decision procedure goes into one of four branches, depending on whether the two Boolean variables `localPriority` for the local buffer and `nsPriority` for the north/south buffer have priority over the east/west buffer. The router model then makes a decision based on the Boolean lock variables. If the local buffer tried to send in the north/south direction, but couldn't due to a conflict or a full buffer, the lock variable `localLns` would become `true`, ensuring that the flit is sent in the same direction next cycle. The probabilistic decisions have probability values marked on the edges. The router then tries to service the buffers in the order listed in the figure. If a buffer fails to win the conflict resolution in sending a flit, it is locked in the same direction and its priority is advanced. Accumulation of *resistiveNoise* is labeled by `RNoise++` when all three buffers send their flits in a cycle. Figure 4 depicts branches 1 and 2 of the four branches. Branch 3 is identical to branch 1, except the order of buffer updates changes from “local, ns, ew” to “ns, ew, local”. Similarly, branch 4 changes branch 2's order from “ew, local, ns” to “local, ew, ns”.

5 Results

All formal models described in this work have been formulated at a higher behavioral level. Therefore, it is necessary to map circuit-level behavior characterizing PSN onto the same behavioral level as these models, in order to quantitatively check PSN related properties. As a major source of PSN, the inductive noise is proportional to the rate of electrical current change in the circuit: abrupt router activity changes in consecutive cycles directly lead to a high rate of current change [16]. A high router activity is characterized as an arbiter servicing all three buffers in a cycle, while a low router activity is when the arbiter services no buffers. PSN is therefore reflected accurately by the frequency of both high-to-low and low-to-high activities over a given timespan. All formal models described in this paper are available on Github⁴. Assuming uniform random flit destination generation at each router, we report verification results for flit injection at the rate of one flit every two clock cycles first, followed by a bursty mode injection. We then report findings of an optimal flit injection pattern that minimizes PSN. All results presented in this section were generated on a machine with an AMD Ryzen Threadripper 12-Core 3.5 GHz Processor and 132 GB memory, running Ubuntu Linux v18.04.3.

We consider the following two transient probabilistic properties: (1) the probability that the number of *resistiveNoise* is lower-bounded by a constant $K \in \mathbb{Z}^+$ within n cycles; and (2) the probability that the total number of *inductiveNoise* is lower-bounded by a constant $K \in \mathbb{Z}^+$ within n cycles. High router activity, characterized by property (1), is a key indicator of local congestion in the network, and a highly congested network leads to high PSN due to an unbalanced

⁴ <https://github.com/formal-verification-research/Modest-Probabilistic-Models-for-NoC>

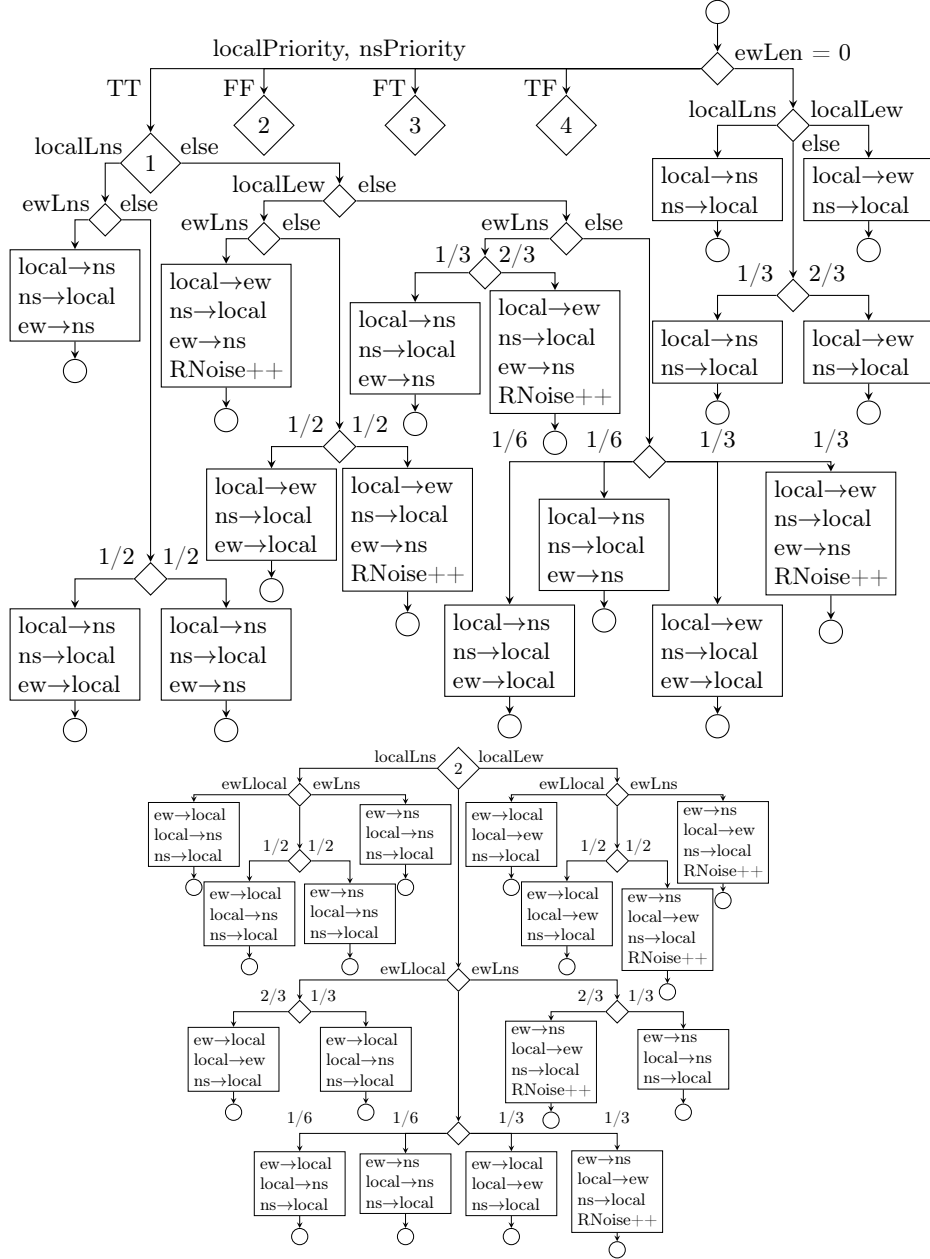


Fig. 4: Decision procedure for the router model after Boolean queue abstraction.

power density [18]. Property (2) reflects an abrupt load change in a router that causes a large inductive drop in the power delivery network [16].

5.1 Every Other Cycle Flit Injection

State Reduction from Abstraction Figure 5 illustrates the impact of applying the aforementioned abstraction techniques on state growth. The exponential cycle-wise growth of the concrete model dramatically reduces to a polynomial growth after Boolean queue abstraction, with other abstraction methods in between. Note that state growth for the presented abstraction techniques are cumulative: probabilistic choice abstraction is applied after predicate abstraction, and it is the base for Boolean queue abstraction. The exponential state growth of the concrete model is due to the probabilistic input. Every other clock cycle, four new flits are generated each with three different possible destinations. This means that if variable x were to increase every other clock cycle, the states, due to just this combination, would be 3^{4x} . This analysis is confirmed by the R^2 values of regression of the state space growth. The R^2 value for the exponential regression is close to 1 for the concrete and predicate abstract models, and the R^2 value for polynomial regression is closest to 1 for both probabilistic choice abstraction and Boolean queue abstraction.

In addition, we also performed exponential and polynomial regression on the state growth of the probabilistic choice and Boolean queue abstractions using only the first ten values to see how accurately each regression would predict the next five values. The polynomial regression was a more accurate prediction of the next five values than the exponential regression. Figure 5 also illustrates the effectiveness of the cumulative abstraction steps detailed in Section 4. No property verification results could be obtained on the concrete model regarding the *resistiveNoise* property, as it is impossible for at least one *resistiveNoise* to occur within the 4 to 5 clock cycles before state explosion occurs. The same reasoning applies to the *inductiveNoise* property.

We keep an integer variable *clk* as a cycle counter, which contributes to the state growth. On the other hand, by gradually increasing its upper bound, state space generation is manageable. This is because state generation only needs to represent model behaviors up to the upper bound of *clk*.

Probabilistic Model Checking (PMC) We used MCSTA, an explicit-state probabilistic model checker, to calculate the probabilities of *resistiveNoise* and *inductiveNoise* occurring within a given bounded number of clock cycles using the final Boolean queue abstraction model. The results are shown in Figure 6. The more abstract models perform an increasing amount of “work”—calculating, communicating, and updating transient and state variables—on every transition. Thus as state space explosion is alleviated, the runtime for state space exploration rises. An attempt to run the Boolean queue abstraction model for 35 clock cycles ran for 22 hours and generated 150.5 million states. When MCSTA attempted to merge these states, it failed due to a segmentation fault indicating an out-of-memory error.

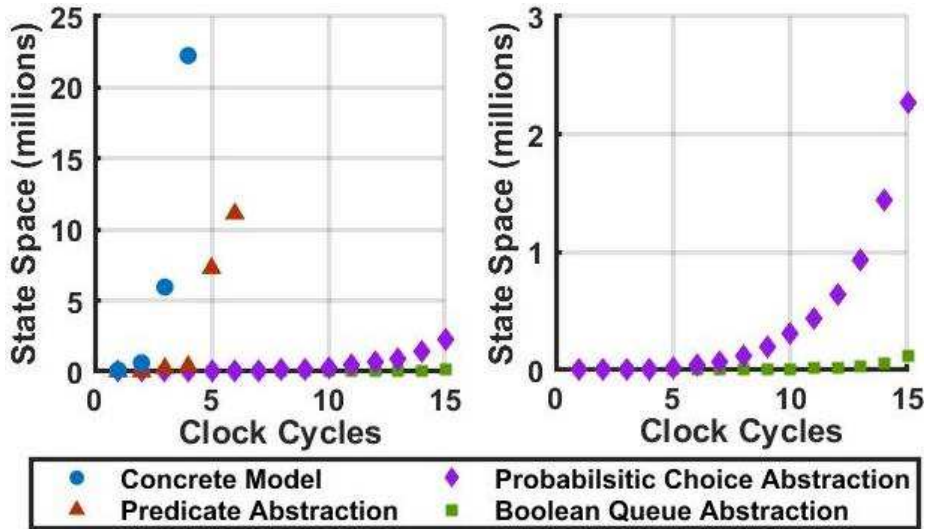


Fig. 5: State count comparison.

Due to the inability of the concrete model to produce any verification results, it is impossible to compare them with abstract models. Comparing the *resistiveNoise* property checking results between the probabilistic choice delay and Boolean queue abstract models, a difference of $1\text{E-}7$, i.e., a 0.15% difference, starts to manifest after 20 clock cycles. It is possible that this difference is due to floating-point error in the transition probabilities, which can be complicated due to the probabilistic behavior of all four arbiters being compounded. These small rounding errors can then accumulate over several clock cycles. With fewer state transitions in the Boolean queue abstracted model, it is possible that the floating-point errors accrue at a different pace. Further research is planned to investigate the minor difference.

Binary decision diagrams (BDDs) have been highly successful in hardware verification [19]. We thus also explored the use of BDD-based symbolic model checking for our NoC models by exporting them to the JANI model interchange format [20] and applying the Storm model checker’s *hybrid* and *dd* engines. Unfortunately, with both supported BDD libraries—CUDD and SYLVAN [21]—Storm quickly ran out of memory. This may be due to probabilistic models requiring multi-terminal BDDs to store probability values, which often does not lead to a memory-efficient representation.

Statistical Model Checking (SMC) Since our models represent DTMC, we can also apply the Monte Carlo simulation-based statistical model checking technique. In contrast to PMC, it avoids state space explosion entirely, but only delivers statistical guarantees and is problematic for rare events. We checked the *resistiveNoise* property at a higher number of cycles using SMC with MODES.

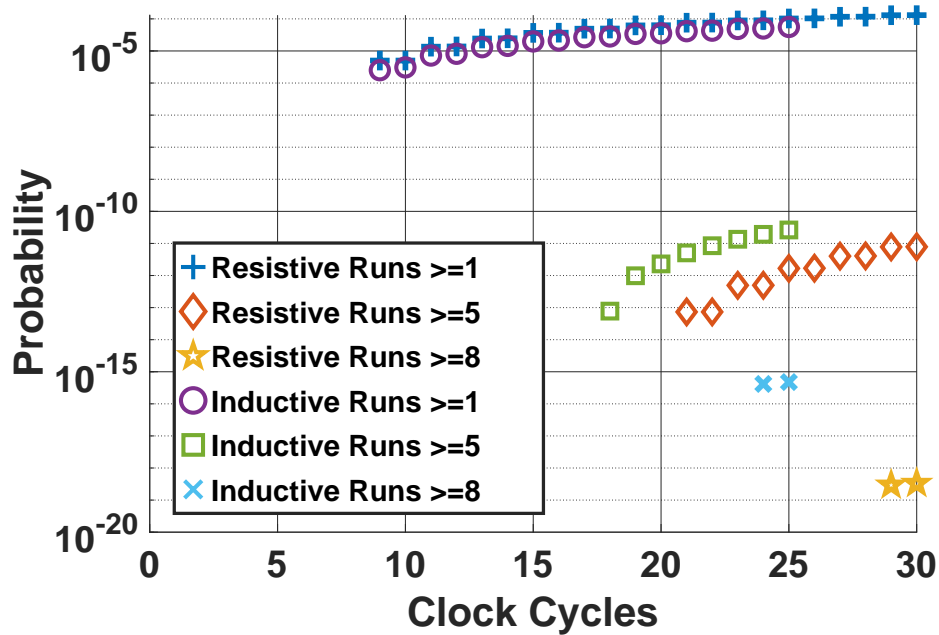


Fig. 6: Probabilities for *resistiveNoise* and *inductiveNoise* in every other cycle input configuration

Running 10000 simulations, MODES reported 643 had at least one optimal run, while 345 had at least one noise run, after 10000 clock cycles. These values correspond to statistical probabilities of 0.0643 and 0.0345 respectively. Due to the rarity of these events, statistical analysis may not provide accurate results.

5.2 Burst Flit Injection

To more accurately model packet injection patterns in real-world applications and measure their impact on PSN, we gathered verification results for a bursty mode packet injection, where for every 10 cycles, the first 3 consecutive cycles each have a flit injected, followed by 7 idle cycles in all four routers. A surprising observation is that this input pattern drastically increases the scalability to allow verification for significantly longer clock cycles. Our analysis indicates that the NoC empties out flits completely within the 7 idle cycles before it receives the next burst of 3 flits. Other than the priority orderings, the NoC has completely reset itself to the initial condition by the end of the idle cycles. Consequently, the number of reachable states is significantly reduced, compared to the every other cycle injection pattern. This reduction leads to the generation of the entire state space for the 2x2 NoC model whereas the clock variable *clk* is no longer used to forcibly stop the model checking after a certain number of cycles as in the every other cycle packet injection pattern. A simple 0 to 9 counter was

added to maintain the 10-cycle injection pattern. Consequently, we made *clk* a *transient* variable in order to continue to check properties in relation to clock cycles. A transient variable is only “live” during the assignments execution when taking a transition, which excludes it from the state vector. In this way, clock cycle progress becomes a *reward* annotation to certain transitions instead of being encoded in the structure of an expanded state space. We can then formalize properties (1) and (2) as reward-bounded reachability queries:

- (1) $\mathbf{P}_{=?}(\diamond^{\text{accumulate}(\text{clk}) \leq N} \text{resistiveNoise} \geq K)$
- (2) $\mathbf{P}_{=?}(\diamond^{\text{accumulate}(\text{clk}) \leq N} \text{inductiveNoise} \geq K)$

Probabilistic model checking of the bursty mode with MCSTA scales to hundreds of clock cycles. In order to prevent the infinite accumulation of *resistiveNoise*, it is upper bounded by 20, resulting in a total of 16,581,401 reachable states explored in about 3.5 hours. Similarly, *inductiveNoise* is upper-bounded by 8, resulting in 10,251,017 states generated in 2.16 hours. A smaller upper bound is required due to the addition of helper variables for accurately tracking the high-to-low and low-to-high activities for *inductiveNoise*.

This input configuration results in only 3 flits every 10 cycles for each arbiter to service in a router, as opposed to 5 for the every-other-cycle injection. However, the ability of each arbiter to receive flits during consecutive cycles has a major impact on the PSN behavior of the NoC. The likelihood of having both *resistiveNoise* and *inductiveNoise* increases significantly. Figure 7 shows the plots of the *cumulative distribution function* (CDF) for *resistiveNoise* being greater than or equal to 1, 5, 10, and 20, and the CDF for *inductiveNoise* being greater than or equal to 1, 5, and 8. Comparing these *resistiveNoise* and *inductiveNoise* probabilities with that of the every other cycle injection shows that PSN is much more likely with bursty style injection, within the same number of clock cycles, despite fewer packets entering the NoC every 10 cycles.

5.3 Flit Generation Pattern to Minimize PSN

We parameterized the bursty mode model so that it could accept a burst lasting any number of cycles, followed by any number of idle cycles. Under our memory constraints, we were able to model check bursts lasting 1, 2, or 3 cycles long, with the requirement that the number of idle cycles must be at least twice as long as the number of cycles in the burst. When testing various burst configurations, we made a critical observation that the input configuration of 1 flit every 3 cycles incurred *zero* probability of an *resistiveNoise* event, and, by extension, zero probability of an *inductiveNoise* event. This is of particular note, because 1 every 3 flit injection results in more flits being injected over time than 3 every 10 injection, but with no occurrence of high-PSN events. Additionally, 1 every 3 flit injection allows considerable number of cycles to be verified compared to every other cycle flit generation and yet it still incurred zero probability of PSN.

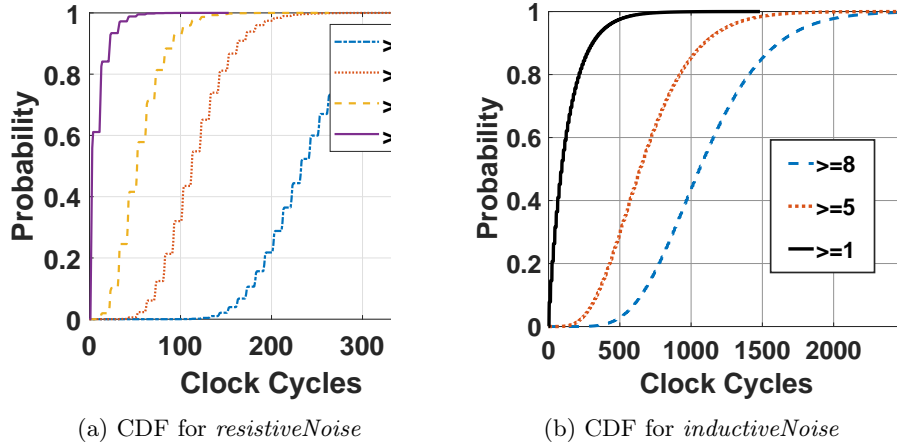


Fig. 7: CDF for *resistiveNoise* and *inductiveNoise* in Burst of Three Input Configuration

5.4 Results Summary and Discussion

The experiments on every other cycle injection suggest that applying PMC on the Boolean queue abstract model is the only viable option to verify PSN related probabilistic properties at longer cycles with reasonable accuracy, given the rarity of the properties. Verification results indicate extremely low probabilities in observing a *resistiveNoise* event within 30 clock cycles. Since *inductiveNoise* accumulates cycles with high-to-low or low-to-high activities, rare occurrences of *resistiveNoise* consequently lead to extremely low probabilities in *inductiveNoise* verification. On the other hand, PMC on the 3 every 10 burst flit injection scales PMC to allow much longer cycles and results in considerably higher PSN due to significantly increased *resistiveNoise* and *inductiveNoise* probabilities. Under our memory constraints, 1 of every 3 flit injection is the most effective packet injection pattern that minimizes PSN probability to zero.

The drastically different PSN behaviors can be explained by analyzing local buffer and arbiter activities of each router. Since the entire NoC only includes four corner routers, each flit has a relatively short distance to its destination router, which reduces the number of buffers it has to visit. Therefore, it is unlikely that all three buffers can contain a flit at the same time, a condition necessary for a *resistiveNoise* cycle to occur. In addition, with X-Y routing, flits tend to exit the NoC quickly without filling up buffers in a way that is conducive to *resistiveNoise*. For the burst mode flit injection, because all three buffers in a router simultaneously start three cycles of burst of flits, it is more likely to incur high router activities and switching between high and low router activities. The burst mode is more prone to cycles of high activity when the NoC has consecutive cycles of flit injection, because it does not have cycles to clear out the buffers before another injection. This causes more traffic in the buffers during the burst,

leading to more cycles of high router activity overall, despite the seven cycles of idle behavior. An optimal compromise is to have 1 flit every 3 cycles where the occurrence of the high PSN events we are tracking reduces to none.

Our findings indicate that spreading flits over a small number of cycles, rather than releasing them in consecutive ones, can drastically reduce PSN. In this work, we made assumption to allow each router to generate flits. In real-world NoC design, network flits are generated and scheduled by external components. Traditional techniques (e.g., IcoNoClast [16]) enhance the router microarchitecture to delay the traversal of flits within a network, thus effectively curbing the maximum noise of the communication fabric. However, such schemes incur additional design complexity and hardware overheads that could be prohibitive for low-power edge applications. Based on our PMC approach, we set a more cost-effective approach to tackling the communication noise in the low-power domains. Our findings suggest that while scheduling network flits, the scheduler should try to insert empty cycles to separate flits in succession in order to minimize PSN.

6 Conclusion

This paper describes our experience in formally modeling a 2×2 NoC system and applying probabilistic verification to quantitatively verify the frequency of PSN. Probabilistic model checking using MCSTA was used to evaluate the properties. The concrete model incurs severe state explosion that prevents property checking. Several abstraction techniques, including a novel probabilistic choice abstraction, are applied to alleviate the rapid state-space explosion and allow for successful verification. Results indicate that bursty flit injection in consecutive cycles yields high likelihood of PSN-causing behavior, while spreading flits over a small number of cycles achieves PSN reduction. This shows that flit injection patterns affect PSN drastically, and that by using certain flit injection patterns, such as 1 flit every 3 cycles, more flits can be injected while also minimizing PSN. For further work, we plan to investigate methods to make the use of BDDs more successful in analyzing this NoC. Additionally, we plan to extend the PSN analysis to larger NoCs, and with different flit generation rates. In order to scale model checking, we plan to pursue the use of assume-guarantee reasoning to combat state explosion. Additionally, we plan to work on a formal proof for the probabilistic choice abstraction.

Acknowledgments. Arnd Hartmanns was supported by NWO VENI grant 639.021.754. Riley Roberts, Benjamin Lewis, Koushik Chakraborty, and Sanghamitra Roy were supported in part by National Science Foundation (NSF) grants CAREER-1253024, CNS-1421022, and CNS-1421068. Any opinions, findings, and conclusions or recommendations expressed in this material are those of the authors and do not necessarily reflect the views of the NSF. Riley Roberts and Benjamin Lewis were supported in part by gift donations from Adobe Systems Incorporated.

References

1. R. Salamat, M. Khayambashi, M. Ebrahimi, and N. Bagherzadeh, “A resilient routing algorithm with formal reliability analysis for partially connected 3D-NoCs,” *IEEE Trans. Computers*, vol. 65, no. 11, pp. 3265–3279, 2016.
2. Z. Zhang, W. Serwe, J. Wu, T. Yoneda, H. Zheng, and C. Myers, “Formal analysis of a fault-tolerant routing algorithm for a Network-on-Chip,” in *Formal Methods for Industrial Critical Systems*, F. Lang and F. Flammini, Eds. Cham: Springer International Publishing, 2014, pp. 48–62.
3. —, “An improved fault-tolerant routing algorithm for a Network-on-Chip derived with formal analysis,” *Science of Computer Programming*, vol. 118, pp. 24 – 39, 2016, Formal Methods for Industrial Critical Systems (FMICS’2014). [Online]. Available: <http://www.sciencedirect.com/science/article/pii/S0167642316000125>
4. F. Verbeek and J. Schmaltz, “On necessary and sufficient conditions for deadlock-free routing in wormhole networks,” *IEEE Transactions on Parallel and Distributed Systems*, vol. 22, no. 12, pp. 2022–2032, 2011.
5. —, “A decision procedure for deadlock-free routing in wormhole networks,” *IEEE Transactions on Parallel and Distributed Systems*, vol. 25, no. 8, pp. 1935–1944, 2014.
6. A. Zaman and O. Hasan, “Formal verification of circuit-switched Network on Chip (NoC) architectures using SPIN,” in *2014 International Symposium on System-on-Chip, SoC 2014, Tampere, Finland, October 28-29, 2014*, 2014, pp. 1–8.
7. Y.-R. Chen, W.-T. Su, P.-A. Hsiung, Y.-C. Lan, Y.-H. Hu, and S.-J. Chen, “Formal modeling and verification for Network-on-Chip,” in *Green Circuits and Systems (ICGCS), 2010 International Conference on*, 2010, pp. 299–304.
8. D. Holcomb, “Formal verification and synthesis for Quality-of-Service in On-Chip Networks,” Ph.D. dissertation, EECS Department, University of California, Berkeley, Dec 2013. [Online]. Available: <http://www2.eecs.berkeley.edu/Pubs/TechRpts/2013/EECS-2013-228.html>
9. H. M. G. Wassel, Y. Gao, J. K. Oberg, T. Huffmire, R. Kastner, F. T. Chong, and T. Sherwood, “Networks on Chip with provable security properties,” *IEEE Micro*, vol. 34, no. 3, pp. 57–68, 2014.
10. J. Sepúlveda, D. Aboul-Hassan, G. Sigl, B. Becker, and M. Sauer, “Towards the formal verification of security properties of a Network-on-Chip router,” in *23rd IEEE European Test Symposium, ETS 2018, Bremen, Germany, May 28 - June 1, 2018*, 2018, pp. 1–6.
11. A. Hartmanns and H. Hermanns, “The Modest Toolset: An integrated environment for quantitative modelling and verification,” in *TACAS*, ser. LNCS, E. Ábrahám and K. Havelund, Eds., vol. 8413. Springer, 2014, pp. 593–598.
12. C. E. Budde, P. R. D’Argenio, A. Hartmanns, and S. Sedwards, “A statistical model checker for nondeterminism and rare events,” in *International Conference on Tools and Algorithms for the Construction and Analysis of Systems*. Springer, 2018, pp. 340–358.
13. C. Dehnert, S. Junges, J.-P. Katoen, and M. Volk, “A storm is coming: A modern probabilistic model checker,” in *Computer Aided Verification*, R. Majumdar and V. Kunčák, Eds. Cham: Springer International Publishing, 2017, pp. 592–600.
14. M. Kwiatkowska, G. Norman, and D. Parker, “PRISM 4.0: Verification of probabilistic real-time systems,” in *Proceedings of the 23rd International Conference on Computer Aided Verification*, ser. CAV’11. Berlin, Heidelberg: Springer-Verlag, 2011, pp. 585–591.

15. B. Lewis, A. Hartmanns, P. Basu, R. J. Shridevi, K. Chakraborty, S. Roy, and Z. Zhang, "Probabilistic verification for reliable Network-on-Chip system design," in *Formal Methods for Industrial Critical Systems - 24th International Conference, FMICS 2019, Amsterdam, The Netherlands, August 30-31, 2019, Proceedings*, ser. Lecture Notes in Computer Science, K. G. Larsen and T. A. C. Willemse, Eds., vol. 11687. Springer, 2019, pp. 110–126. [Online]. Available: https://doi.org/10.1007/978-3-030-27008-7_7
16. P. Basu, R. J. Shridevi, K. Chakraborty, and S. Roy, "IcoNoClast: Tackling voltage noise in the NoC power supply through flow-control and routing algorithms," *IEEE Trans. VLSI Syst.*, vol. 25, no. 7, pp. 2035–2044, 2017.
17. R. J. Shridevi, D. M. Ancajas, K. Chakraborty, and S. Roy, "Tackling voltage emergencies in NoC through timing error resilience," in *ISLPED*, 2015, pp. 104–109.
18. N. Dahir, T. S. T. Mak, F. Xia, and A. Yakovlev, "Modeling and tools for power supply variations analysis in Networks-on-Chip," *TC*, vol. 63, no. 3, pp. 679–690, 2014.
19. S. Chaki and A. Gurfinkel, "BDD-based symbolic model checking," in *Handbook of Model Checking*, E. M. Clarke, T. A. Henzinger, H. Veith, and R. Bloem, Eds. Springer, 2018, pp. 219–245.
20. C. E. Budde, C. Dehnert, E. M. Hahn, A. Hartmanns, S. Junges, and A. Turrini, "JANI: Quantitative model and tool interaction," in *23rd International Conference on Tools and Algorithms for the Construction and Analysis of Systems (TACAS)*, ser. Lecture Notes in Computer Science, A. Legay and T. Margaria, Eds., vol. 10206, 2017, pp. 151–168.
21. T. van Dijk and J. van de Pol, "Sylvan: multi-core framework for decision diagrams," *STTT*, vol. 19, no. 6, pp. 675–696, 2017.